

1 **Arabian Red Sea coastal soils as potential mineral dust sources**

2 **P. Jish Prakash¹, Georgiy Stenchikov¹, Weichun Tao¹, Tahir Yapici¹, Bashir Warsama¹,**
3 **and Johann Engelbrecht^{2,1}**

4 [1] King Abdullah University of Science and Technology (KAUST), Physical Science and
5 Engineering Division (PSE), Thuwal, 23955-6900, Saudi Arabia.

6 [2] Desert Research Institute (DRI), Reno, Nevada 89512-1095, U.S.A.

7 Correspondence to P. Jish Prakash (jishprakash@gmail.com)

8

9 **Co-Editor Decision**

10 **Co-Editor Decision: Publish subject to technical corrections** (05 Sep 2016) by Paola Formenti

11 **Comments to the Author:**

12 Dear authors, thank you for taking the referees' suggestions into account. The manuscript can be
13 published once you have incorporated the necessary corrections. I urge you to make sure that all the
14 relevant references are included. best regards.

15

16 **Authors Response**

17 We perused the manuscript to ensure that all the references are included. Two corrections were
18 made (see comments below), and we also made other minor corrections throughout the
19 manuscript. The most important are highlighted below.

20 Regards

21

22

1 **Abstract**

2 Both Moderate Resolution Imaging Spectroradiometer (MODIS) and Spinning Enhanced Visible
3 and InfraRed Imager (SEVIRI) satellite observations suggest that the narrow heterogeneous Red
4 Sea coastal region is a frequent source of airborne dust that, because of its proximity, directly
5 affects the Red Sea and coastal urban centers. The potential of soils to be suspended as airborne
6 mineral dust depends largely on soil texture, moisture content, and particle size distributions.
7 Airborne dust inevitably carries the mineralogical and chemical signature of a parent soil. The
8 existing soil databases are too coarse to resolve the small but important coastal region. The purpose
9 of this study is to better characterize the mineralogical, chemical and physical properties of soils
10 from the Red Sea Arabian coastal plane, which in turn will help to improve assessment of dust
11 effect on the Red Sea and land environmental systems and urban centers. Thirteen surface soils
12 from the hot-spot areas of wind-blown mineral dust along the Red Sea coastal plain were sampled
13 for analysis. Analytical methods included Optical Microscopy, X-ray diffraction (XRD),
14 Inductively Coupled Plasma Optical Emission Spectrometry (ICP-OES), Ion Chromatography
15 (IC), Scanning Electron Microscopy (SEM), and Laser Particle Size Analysis (LPSA). We found
16 that the Red Sea coastal soils contain major components of quartz and feldspar, as well as lesser
17 but variable amounts of amphibole, pyroxene, carbonate, clays, and micas, with traces of gypsum,
18 halite, chlorite, epidote and oxides. The range of minerals in the soil samples was ascribed to the
19 variety of igneous and metamorphic provenance rocks of the Arabian Shield forming the
20 escarpment to the east of the Red Sea coastal plain. The analysis revealed that the samples contain
21 compounds of nitrogen, phosphorus and iron that are essential nutrients to marine life. The
22 analytical results from this study will provide a valuable input into dust emission models used in
23 climate, marine ecology, and air-quality studies.

24 **Key words:** Dust mineralogy; Dust chemistry; Soil samples; Saudi Arabian dust

25 **1. Introduction**

26 Mineral dust is the most abundant atmospheric aerosol, primarily suspended from soils in arid and
27 semi-arid regions of the globe (Buseck et al., 1999; Washington and Todd, 2005; Goudie and
28 Middleton, 2006; Muhs et al., 2014), including deserts of the Arabian Peninsula (Edgell, 2006).
29 Dust aerosols profoundly affect climate, biogeochemical cycles in the ocean and over land, air-
30 quality, atmospheric chemistry, cloud formation, visibility, and human activities (Prospero et al.,

1 2002;Haywood and Boucher, 2000;Hsu et al., 2004;Sokolik and Toon, 1999;Kumar et al., 2014;De
2 Longueville et al., 2010;Jickells et al., 2005;Mahowald, 2009;Huang et al., 2006;Huang et al.,
3 2014;Fryrear, 1981;Nihlen and Lund, 1995;Hagen and Woodruff, 1973;Bennett et al.,
4 2006;Bennion et al., 2007;Twomey et al., 2011;Wang et al., 2010). The Arabian Peninsula is one
5 of Earth's major sources of atmospheric dust, which contributes as much as 11.8% (22 – 500 Mt/a)
6 of the total (1,877–4000 Mta⁻¹) global dust emissions (Tanaka and Chiba, 2006). The Red Sea
7 surrounded by African and Arabian deserts is strongly affected by dust. Along with profound
8 impact on the surface energy budget over land and the sea (Brindley et al., 2015;Kalenderski et
9 al., 2013;Osipov et al., 2015), dust is an important source of nutrients especially for the
10 oligotrophic northern Red Sea region (Acosta et al., 2013). Dust affects marine life, also
11 controlling incoming solar and terrestrial radiation. The coastal plains of the Arabian Peninsula
12 along the Red Sea and Persian Gulf are among the most populated areas in this region hosting the
13 major industrial and urban centers.

14 Both Moderate Resolution Imaging Spectroradiometer (MODIS) and Spinning Enhanced Visible
15 and InfraRed Imager (SEVIRI) satellite observations suggest that the narrow Red Sea coastal belt
16 is an important dust source region, augmented by the fine-scale sediment accumulations, scattered
17 vegetation, and variable terrain. Dust hot spots are located within the narrow coastal region, and
18 because of their proximity to the Red Sea, contribute to the dust/nutrient balance of the sea, during
19 both dusty and fair weather conditions.

20 Dust emission rates from soils and sites of airborne particles strongly depend on the soil particle
21 size distributions. Optical properties such as scattering, absorption and refractive indices vary by
22 mineralogical content and particle size of the dust in the atmosphere. Dust reactivity in the seawater
23 also depends on their mineralogy, e.g. carbonates (calcite, dolomite), evaporites (gypsum) and
24 some oxides (hematite, goethite) are generally more soluble in water than for example most
25 silicates (quartz, feldspars, micas, clays, amphiboles, pyroxenes). Soils in arid regions are most
26 susceptible to wind erosion, where particles are only loosely bound to the surface by the low soil
27 moisture or being physically disturbed by agriculture or traffic. Dust uplifting occurs in a source
28 region when the surface wind speed exceeds a threshold velocity (Gillette and Walker, 1977),
29 which is a function of surface roughness elements, grain size, and soil moisture (Marticorena and
30 Bergametti, 1995;Wang et al., 2000). Fine soil particles that can be transported over large distances

1 are released by saltating coarse silt and sand particles (Caquineau et al., 1997). Soil morphology,
2 mineralogy, and chemical composition define the abundance and composition of airborne dust,
3 however, not directly but through the series of complex fine-scale non-linear processes.

4 From preliminary observations it is estimated that 5 to 6 major dust storms per year impact the
5 coastal region of Saudi Arabia, depositing about 6 Mt of mineral dust into the Red Sea (Prakash et
6 al., 2015). Simulations and satellite observations suggest that the coastal dust contribution to the
7 total deposition flux into the Red Sea could be significant even during fair weather conditions
8 (Jiang et al., 2009). However, the mineralogy, physical properties, and chemical composition of
9 dust generated from the Red Sea coastal region remain uncertain. The coastal plain is a narrow
10 geographically and petrographically heterogeneous piedmont area, and existing soil databases do
11 not provide the spatial resolution for the region to be adequately described (Nickovic et al., 2012).
12 The importance of keeping track of dust mineralogy during the atmospheric transport was recently
13 recognized and implemented in the models (Perlwitz et al., 2015b, a). Equation (1) relates the size-
14 dependent soil dust properties with that emitted to the atmosphere, where dust size-distribution
15 and compositional characteristics are further adjusted, as dust particles atmospheric residence time
16 depends on their particle size distribution and particle mass. To explain the connection between
17 soil properties and airborne dust abundance and composition we discuss the physically-based dust
18 generation parameterizations currently used in the advanced modeling systems (Grell et al.,
19 2005; Zender et al., 2003). The vertical mass flux F_j ($\text{kgm}^{-2}\text{s}^{-1}$), of dust size component j , generated
20 from the ground into the atmosphere can be assessed as follows:

$$21 \quad F_j = TSf_m\alpha Q_s \sum_{i=1}^I M_{ij} \quad (1)$$

22 Where, T is a tuning constant for adjusting to different horizontal and temporal resolutions. The
23 parameter “ S ” is the erodibility factor that accounts for the susceptibility of a landscape to wind
24 erosion controlled by the non-erodible roughness elements and the erodibility of soils within the
25 erodible area of a landscape (Webb and Strong, 2011). This parameter is often defined via the so-
26 called “source function” that accounts for the spatial distribution of dust source intensities based
27 on a variety of algorithms (Menut et al., 2013). The parameter f_m is a grid cell fraction of exposed
28 bare soil suitable for dust mobilization. The coefficient “ α ” is sandblasting mass efficiency
29 determined by the mass fraction of clay particles in the soil. The parameter Q_s is the total
30 horizontally saltation mass flux ($\text{kgm}^{-1}\text{s}^{-1}$), which is proportional to the third power of friction

1 velocity (u^*_s) when it exceeds a threshold velocity u^*_t (Oleson et al., 2010; Zender et al., 2003). In
2 dust emission models, the soil erodibility is represented through the effects of soil texture and
3 moisture content on the threshold friction velocity u^*_t and the aerodynamic roughness length f_z
4 (Oleson et al., 2010; Webb and Strong, 2011). “ $M_{i,j}$ ” is the mass fraction of each source mode i ,
5 carried in each transport bin j .

6 The sample area in this study lies within the approximately 60–70 km wide Tihāmah coastal plain,
7 comprised of the Tihāmat Asīr in the south and the Tihāmat Al-Hejaz to the north. The plain is
8 bounded by the Red Sea in the west, with the mountains of Midyan, Ash Shifa and Asir forming
9 an escarpment to the east (Edgell, 2006), with few breaks in the mountains in the northwest. The
10 mountains form a 1,000–3,000 m elevation Red Sea escarpment, comprised of igneous,
11 metamorphic and volcanic rocks of variable age, from Pre-Cambrian (1,000–545 Ma) to the less
12 than 30 Ma in age (Grainger, 2007). The Red Sea rift basin itself is overlain by the much younger
13 sediments of Quaternary age (< 2.6 Ma).

14 Al-Farraj (2008) studied the soils from the Jazan region of southern Saudi Arabia, identifying
15 smectite, kaolinite and illite as the predominant clay minerals, together with lesser amounts of
16 chlorite, quartz and feldspars. Shadfan et al. (1984) investigated mineralogical content and general
17 characteristics of soils from some agricultural areas in Saudi Arabia. They found carbonate, quartz
18 and gypsum to be the main constituents of the sand and silt fractions in soils of the eastern region,
19 while quartz, carbonate and feldspars dominate soils in the central region. The soils in the west
20 contain mainly quartz, feldspars, hornblende and mica. Palygorskite was found to be the main clay
21 mineral in soils in the eastern region, kaolinite in the central region, and kaolinite, smectite and
22 mica in the western region. Aba-Husayn et al. (1980) mineralogically analyzed soils from the
23 southwestern region of Saudi Arabia, along the mountainous Asir region between Mecca and
24 Abha. They found major amounts of quartz, feldspars and micaceous minerals in the silt fractions,
25 with the clay-size fractions of kaolinite, smectite, and vermiculite, with kaolinite in the well-
26 drained highland areas. Viani et al. (1983) studied fourteen soils from alluvial basins in the Wadi
27 ad Dawasir, and Wadi Najran areas of southwestern Saudi Arabia. Due to the fact that the alluvial
28 clay-size fractions were from weathered igneous rocks of the surrounding mountains, they were
29 found to be composed largely of smectite, mica, kaolinite, chlorite, palygorskite and vermiculite.
30 With the exception of the area around Jazan in the south, which is impacted by the Indian Ocean

1 monsoon, the Red Sea coastal region has a desert climate characterized by extreme heat, reaching
2 39 °C during the summer days, with a drop in night-time temperatures of about 10 °C. Although
3 the extreme temperatures are moderated by the proximity of the Red Sea, in summer the humidity
4 is often 85% or higher during periods of the northwesterly *Shamal* winds. Annual rainfall
5 diminishes from an annual average of 133 mm at Jazan to 56 mm at Jeddah, and 24 mm at Tabuk
6 in the north. Vegetation is sparse, being restricted to semi-desert shrubs, and acacia trees along the
7 ephemeral rivers (wadis), providing forage for small herds of goats, sheep and dromedary camels.
8 During infrequent but severe rainstorms, run-off from the escarpment along wadis often produce
9 flash floods. With such events, fine silt and clays are deposited on the coastal plain, which are
10 transformed into dust sources during dry and windy periods of the year. The resultant dust is
11 transported and deposited on the coastal plain and adjacent Red Sea by prevailing northwesterly
12 to southwesterly winds, with moderate breezes (wind speed $>5.5 \text{ ms}^{-1}$) from the north
13 (<http://www.windfinder.com/weather-maps/report/saudi-arabia#6/22.999/34.980>).

14 2. Objectives

15 The assumption is that at least part of the dust in the ambient atmosphere in the coastal region is
16 from windblown and otherwise disturbed soils along the Red Sea coast. Jiang et al. (2009) and
17 Kalenderski et al. (2013) found that the coastal area emits about 5–6 Mt of dust annually. Due to
18 its close proximity, a significant portion of this dust is likely to be deposited to the Red Sea, which
19 could be comparable in amount to the estimated annual deposition rate from remote sources during
20 major dust storms (Prakash et al., 2015).

21 Due to the limited compositional information of soils along the Red Sea coastal region, this study
22 aims to provide mineralogical, chemical, and morphological information on soils (Scheuven and
23 Kandler, 2014) within the central part of the Red Sea coastal plain of Saudi Arabia, (Fig. 1).

24 This information will help to better quantify the ecological impacts, health effects, damage to
25 property, and optical effects of dust blown from these areas (Engelbrecht et al., 2009a, b; Weese
26 and Abraham, 2009). The mineralogical compositions of the soils tie into that of the parental rocks,
27 weathering conditions and time. This research will also complement soil and dust studies
28 performed in the Arabian Peninsula as well as globally (Engelbrecht and Moosmüller,
29 2014; Engelbrecht et al., 2009b). Knowledge of the mineralogy of the soils will provide data on

Commented [JE1]: Reference added

1 refractive indices, particle size and shape parameters, which can be used to calibrate dust transport
2 models, and help to assess the impact of dust events on the coastal plain and the Red Sea.

3 **3. Sampling and analysis**

4 A total of thirteen samples was collected at four localities along the Red Sea coastal plain (Fig. 1).
5 Three samples (S1–S3) collected at 25 km northeast of Mastorah near washland of Wadi Hazahiz
6 located 26 km from Red Sea. Samples (S4–S6) collected at 30 km east of Ar Rayis near Ushash,
7 which is a village in Al Madinah province located 32 km from Red Sea. Samples (S7–S9) collected
8 at 27 km north of Yanbu at washland of Wadi al Wazrah with an elevation of 158 m above sea
9 level and located 30 km from Red Sea. Four samples (S10–S13) collected at 28 km southwest of
10 Mecca near Wadi An Numan located 45 km from Red Sea. The coordinates of the sample sites are
11 provided in Table 1. All thirteen samples can be classed as Leptosols (Regosols)
12 (<http://www.fao.org/ag/agl/agll/wrb/soilres.stm>).

13 The grab soil samples collected in the field were sieved to < 1 mm to remove pebbles, plant
14 material and other detritus. Where necessary, they were air-dried in the laboratory, before being
15 labeled, catalogued and stored in capped plastic bottles. Sub-sets of these samples were screened
16 to $< 38 \mu\text{m}$ for mineral analysis by X-ray powder diffraction (XRD), chemical analysis, and
17 Scanning Electron Microscopic (SEM) based individual particle analysis. Further samples of > 75 ,
18 $< 125 \mu\text{m}$ were sieved for mineralogical investigation by optical microscopy, and $< 600 \mu\text{m}$ for
19 Laser particle size analysis (LPSA).

20 Petrographic microscopy is particularly suited to the optical identification of mineral grains larger
21 than about $10 \mu\text{m}$ (Kerr, 1959). It remains a cost effective and accurate technique to obtain
22 mineralogical information which is otherwise difficult to obtain, e.g. the identification of feldspars,
23 amphiboles and pyroxenes. The > 75 , $< 125 \mu\text{m}$ sieved soil fraction grains were mounted in epoxy
24 on a glass slide and ground to a thickness of approximately $30 \mu\text{m}$, for transmitted light optical
25 microscopy. Minerals with distinctive optical properties, including refractive indices,
26 birefringence, extinction angles, pleochroism, and optical interference patterns, or those showing
27 twinning, distinctive cleavage, and diagnostic extinction angles, can be readily be identified by
28 optical microscopy (Kerr, 1959). Minerals readily identified in these samples by this method
29 include quartz, various feldspars, amphiboles, pyroxenes, micas and carbonates. However,

1 depending on the mineral type, particles < 10 µm in diameter are often difficult to identify by this
2 method, including clay minerals and other layered silicates. The method is biased towards easily
3 identifiable and coarser minerals, especially those with twinning such as feldspars, and showing
4 color and pleochroism such as hornblende and biotite. The method, although one of the most
5 practical for qualitative mineral analysis, does require mineralogical expertise.

6 X-ray diffraction (XRD) is a non-destructive technique for characterization of minerals. Powder
7 XRD is particularly suited for fine-grained crystalline mineral mixtures, <10 µm in diameter. The
8 procedure measures the crystallinity of a sample, i.e. excludes amorphous phases such as clay-like
9 colloids (Formenti et al., 2011;Leinen et al., 1994;Engelbrecht et al., 2016;Kandler et al., 2009),
10 partly crystalline layered silicates such as some clays, and hydroxides. If an amorphous phase is
11 present, it will not be fingerprinted by XRD. The assessment of mineral content of a powder sample
12 by the relative intensity ratio (RIR) method suggested by Chung (1974), and as applied in our
13 measurements, does not account for amorphous content. Dust reactivity in the seawater as well as
14 optical properties depend on their mineralogy, e.g. carbonates and some silicates are generally
15 more soluble in water than for example feldspars, amphiboles, pyroxenes or quartz. A Bruker D8®
16 X-ray powder diffraction (XRD) system was used to analyze the mineral content of the soil
17 samples. The diffractometer was operated at 40 kV and 40 mA, with Cu K α radiation, scanning
18 over a range of 4° to 50° 2 θ . The Bruker Topas® software using the relative intensity ratio (RIR)
19 method was applied for semi-quantitative XRD analyses of the < 38 µm screened dust samples
20 (Rietveld, 1969;Chung, 1974;Esteve et al., 1997;Caquineau et al., 1997;Sturges et al., 1989).

21 Laser particle size analysis (LPSA) was performed on the thirteen soil samples. The LPSA system
22 measures the size-class fractions of a soil or sediment sample in an aqueous suspension, based on
23 the principle that light scatters at angles inversely proportional to, and with intensity directly
24 proportional to particle size (Gee and Or, 2002). The grab samples were sieved to < 600 µm before
25 being introduced to the laser analyzer (Micromeritics Saturn DigiSizer 5200®) in an aqueous
26 solution of 0.005% surfactant (sodium metaphosphate). The suspensions were internally dispersed
27 by applying ultra-sonication, before being circulated through the path of the laser light beam. The
28 measured size-class fractions were grouped as clay (< 2 µm), silt (> 2, < 62.5 µm) and sand (>
29 62.5, < 600 µm), (Engelbrecht et al., 2012). This analytical method disperses soil aggregates which
30 are potential dust particles, so shifting the particle size distribution curves towards the smaller

1 particle sizes. This may introduce a bias into the actual size distribution of wind generated dust
2 particles in the field.

3 The < 38 µm sieved samples were chemically analyzed for elemental composition by Inductively
4 Coupled Plasma Optical Emission Spectrometry (ICP-OES), and their water soluble ions by Ion
5 Chromatography (IC). For ICP-OES, splits of 0.1 g of each of the samples were digested in a 1:3:1
6 mixture of concentrated HF, HCl and HNO₃, in a microwave oven (Milestone Ethos1[®]) operated
7 at a temperature up to 195 °C for 15 minutes. The solutions were diluted from 25 ml to 250 ml
8 before being analyzed on the ICP-OES (Varian 720-ES[®]), for Na, Mg, Al, Si, P, S, K, Ca, Ti, V,
9 Cr, Mn, Fe, Co, Ni, Cu, Zn, Sr, Cd, Ba and Pb. The accuracy of the analyses was monitored by
10 analyzing the National Institute of Standards and Technology (NIST) standard reference material
11 1646a with each batch of soil samples. The elemental composition of dust *per se* does not provide
12 adequate information on its mineral content. However, with *a priori* knowledge of the mineral
13 composition of the samples, from optical and XRD measurements, “normative” mineral
14 compositions can be calculated. This provides a method for inter-comparing chemically analyzed
15 samples with each other.

16 Further splits (~ 0.01 g) of the < 38 µm sieved samples were sonicated in 15 ml of de-ionized
17 distilled water, the suspension left to settle overnight, and the extractions analyzed by IC
18 (DIONEX ICS-3000[®]). The water soluble cations of sodium (Na⁺), potassium (K⁺), calcium (Ca²⁺)
19 and magnesium (Mg²⁺), and anions of sulfate (SO₄²⁻), chloride (Cl⁻), phosphate (PO₄³⁻) and nitrate
20 (NO₃⁻) were analyzed by this method.

21 Electron microscopy provides information on the individual particle size, shape, chemical
22 composition, and mineralogy of micron-size particles, important for determining the optical
23 parameters for modeling of dust (Moosmüller et al., 2012). The individual particle chemistry,
24 especially of the soluble minerals such as carbonates, is often of importance in medical geology
25 and to marine life. The Scanning Electron Microscope (SEM) based individual particle analysis
26 was performed on the < 38 µm sieved sample splits. A dual approach was followed, the first being
27 the computer controlled scanning electron microscopy (CCSEM) and the second, secondary
28 electron imaging by high resolution scanning electron microscopy (SEM). For each sample, a
29 portion of soil was suspended in isopropanol and dispersed by sonication. The suspension was

Commented [JE2]: We removed the element names and retained only the symbols

1 vacuum filtered onto a 0.2 μm pore size polycarbonate substrate. A section of the substrate was
2 mounted onto a metal SEM stub with colloidal graphite adhesive. The sample mounts were sputter-
3 coated with carbon to dissipate the negative charge induced on the sample by the electron beam.
4 The automated CCSEM analysis was conducted on a Tescan MIRA 3[®] field emission scanning
5 electron microscope (FE-SEM). The CCSEM analysis was performed by rastering the electron
6 beam over the sample while monitoring the resultant combined backscattered electron (BE) and
7 secondary electron (SE) signals. The BE intensities were applied to set grayscale levels, to
8 distinguish particles of interest from background. The system was configured to automatically
9 measure the size and the elemental composition for about 2,000 individual particles of $> 0.5, < 38$
10 μm sizes. Individual particles were classified into particle types according to their elemental
11 compositions. A digital image was acquired of each particle, for measurement, and stored for
12 subsequent review. Size measurements were based on diameters obtained from the projected area
13 of each particle, by tracing their outer edges. Compositional information was determined through
14 collection and processing of characteristic X-rays by energy dispersive spectroscopy (EDS) using
15 a silicon drift detector. The elements identified in the spectrum were processed to obtain their
16 relative concentrations. The particles were grouped into “bins” by their particle size and chemical
17 ratios. From the chemical measurements, and *a priori* knowledge of the sample mineralogy (from
18 optical microscopy and XRD), the mineralogy of individual particles can often be inferred, e.g. Si
19 particles being quartz, Ca particles being calcite, Ca plus S particles being gypsum. Due to the
20 attenuation of the electron beam as it impinges the particle surface and loss of energy, the analysis
21 is physically limited to an electron interaction volume of 2–5 μm below the mineral surface,
22 depending on the primary beam voltage and the mineral density (Goldstein et al., 2003). Most of
23 the investigated mineral dust particles have coatings of clay minerals and oxides, which results in
24 an overestimation of the amounts of these minerals when analyzed by CCSEM (Engelbrecht et al.,
25 2009a;Engelbrecht et al., 2016;Engelbrecht et al., 2009b).

26 The field emission electron source allows for high magnifications and sharp secondary electron
27 images (SEI). This technique allows for the detailed study of particle shape, surface features, and
28 chemical compositions. Approximately five SEIs with energy dispersive spectra (EDS) for each
29 of the thirteen samples were collected. Supplement S03 shows few SEM SEIs and EDS spectra of
30 the $< 38 \mu\text{m}$ soil particles from the sampling site.

1 **4. Results**

2 **4.1 Particle Size Analysis**

3 Particle volume size plots of the < 600 μm sieved samples are listed in Table 2 and graphically
4 presented in Fig. 2. The thirteen soils are composed of on average close to 89% sand fractions.
5 Also, the silt makes up approximately 10% and the clay on average less than 1.5% of the sample
6 volume.

7 Field and laboratory measurements on dust from the western USA. (Engelbrecht et al., 2012)
8 showed that dust emissions are largely controlled by their soil particle size distributions (Kok,
9 2011b, a). It was established that surface soils with a silt content of greater than about 50% and a
10 clay content of less than about 10%, i.e. samples in the “silt loam” field (Fig. 2) have the greatest
11 potential to become re-suspended in the air and to generate airborne mineral dust. This particle
12 size criterion provides an important measure for whether a site or region has the potential to be a
13 significant dust source (Greely and Iversen, 1985). These include soils from previously identified
14 dust sources such as Bodélé Depression (Washington et al., 2003), loess along the Danube River
15 valley, Kuwait, China (Engelbrecht and Moosmüller, 2014), silt deposits collected on
16 Fuerteventura Island assumed to contain dust from the western Sahara (Menéndez et al., 2014), as
17 well as one diatomaceous silt sample from Reno, USA. Besides the particle size distribution it was
18 shown that moisture content and surface roughness play important roles in the saltation and de-
19 segregation of soil particles (Marticorena, 2014). Judging from their particle size distributions
20 alone, soil samples collected from the coastal zone of Saudi Arabia are not considered to contain
21 enough silt-size particles to be efficient emitters of dust. However, the satellite images show that
22 these coastal dust sources are activated quite frequently.

23 **4.2 Optical microscopy**

24 Mineralogical investigation by optical microscopy of three > 75, < 125 μm sieved samples showed
25 them to consist of partially weathered angular mineral grains in sediments probably eroded from
26 the Pre-Cambrian basement and Tertiary volcanic rocks of the Arabian Shield, approximately 50
27 km to the east of the Red Sea coastline (Edgell, 2006). The major minerals identified in this size
28 range are feldspar (mainly plagioclase), quartz, pyroxene (aegerine-augite), amphibole, and mica

1 (biotite, muscovite). Lesser amounts of potassium feldspar (orthoclase, microcline), carbonates
2 (calcite, dolomite), chlorite, epidote and oxides were identified by optical microscopy.

3 **4.3 XRD mineral analysis**

4 XRD analysis of the thirteen, < 38 µm sieved samples (Fig. 3) from the Red Sea coastal plain
5 confirmed variable mass percentages of quartz (19–44%) and feldspars (plagioclase, K-feldspar)
6 (31–48%), as well as of amphibole (and pyroxene) (4–31%), lesser amounts of calcite (0.4–6.2%),
7 dolomite (1.9–6.6%), clays (smectite, illite, palygorskite, kaolinite) and chlorite (3.3–8.3%), with
8 traces of gypsum (0–0.6%) and halite (0.2–4.8%). The average amphibole (plus pyroxene) content
9 for the four samples taken at the southernmost locality (Fig. 1, S10–S13) is substantially higher
10 than for the nine samples taken at the other three localities (Fig. 1, S1–S9), being approximately
11 26% for the former and 11% for the later. For this and other localities, the mineralogy resembles
12 that of the igneous and metamorphic rocks of the adjacent mountainous escarpment and Arabian
13 Shield (Edgell, 2006). This can be attributed to differences in the mineral composition of the
14 Arabian Shield rocks, distance of the sampling sites from the source regions, and the extent of
15 weathering in the surface soils.

16 **4.4 Chemistry (ICP-OES and IC)**

17 Chemical analysis of the < 38 µm sieved bulk samples by ICP-OES and IC are presented in
18 Appendix A, Tables A1 and A2 and a plot of the major elements expressed as oxides, shown in
19 Fig 4. The soils are of reasonably consistent chemical composition throughout the sampled region.

20 The sedimentary samples all contain major mass percentages of SiO₂, varying between 63% and
21 78% in the thirteen samples, mostly as the mineral quartz, and lesser mass percentages of Al₂O₃,
22 CaO, Na₂O, and K₂O, in plagioclase and potassium feldspars. SiO₂ together with Al₂O₃, Fe₂O₃,
23 TiO₂, MnO, MgO, and some K₂O is also contained in the previously identified clays, micas and
24 amphiboles. Small amounts of CaO (0.9–1.7%) are contained in gypsum and calcite, and together
25 with MgO (2.3–3.1%) in dolomite.

26 The water soluble ions account for a small percentage of the total mass of the soils, varying
27 between 0.1% and 0.7% for the total cations, and 0.03% and 0.8% for the total anions. These
28 account primarily for calcite and dolomite (~ 0.3%), and gypsum (~ 0.2%), with even lesser

1 amounts of halite and other chlorides from sea salt. This unexpectedly low concentration of halite
2 and other soluble salts in the soils of the coastal plains can be ascribed to the fact that all the
3 samples were collected at distances varying between 21 and 42 km from the Red Sea coast, and
4 the absence of local playas or other saline soils close to the four sampled areas. It is also expected
5 that the salts had been leached from the soil samples collected from surface. Also of importance
6 to dust-borne nutrients likely to be deposited in the Red Sea, is the low concentration of water
7 soluble PO_4^{3-} (avg. 0.003 %) in comparison to the total P_2O_5 (avg. 0.4%) in the soils. The
8 phosphorus is largely bound in the low soluble mineral apatite (francolite), commonly found in
9 the sediments throughout the Arabian Peninsula.

10 The Fe/Al mass ratios for the suite of 13 samples from the Red Sea coastal plain vary between
11 1.26 and 3.59, with a geometric mean 2.41 (Appendix A). These measurements partly overlap with
12 the Fe/Al ratios of 0.53 – 1.71 measured for dust samples from the Bodélé Depression in Chad
13 (Bristow et al., 2010), and included in the range of 0.41 – 3.78 for re-suspended soil samples from
14 global dust sources (Engelbrecht et al., 2016). In contrast, soil samples collected from ferricretes
15 along the southern Sahel in northern Africa have Fe/Al ratios in the range of 2.95 to 3.43 (Roquin
16 et al., 1990).

17 **4.5 SEM chemical analysis**

18 Approximately 2000 individual dust particles per sample in the 0.5–38 μm size range were
19 analyzed automatically by CCSEM, for chemical composition, particle morphology and size. The
20 particles were classed into 14 bins as per their chemical compositions. Mineral labels were
21 assigned to these chemical bins, e.g. Fe-rich as hematite (Fe_2O_3) (also possibly goethite, magnetite
22 or ferrihydrite), Ca-S rich as gypsum ($\text{CaSO}_4 \cdot 2\text{H}_2\text{O}$), Ca-Mg rich as dolomite ($\text{CaMg}(\text{CO}_3)_2$), Ca
23 rich as calcite (CaCO_3), Ca-Al-Si rich as anorthite ($\text{CaAl}_2\text{Si}_2\text{O}_8$), Na-Al-Si rich as albite
24 ($\text{NaAlSi}_3\text{O}_8$), K-Al-Si rich as K-feldspar (KAlSi_3O_8), and Si-rich as quartz (SiO_2). The CCSEM
25 results for the 0.5–38 μm analyzed set as well as the 0.5–2.5 μm (fine) subset are presented in Fig.
26 5 and 6.

27 For the total data set, the samples in the 0.5–38 μm size range contain by mass about 0.1–10.2%
28 quartz, 5–54% feldspar, 45–72% clay minerals, as major components with lesser amounts of
29 calcite, dolomite, gypsum, and iron oxides. The clay minerals can occur as individual minerals but

1 largely as coatings on other silicates (Engelbrecht et al., 2009a). The 0.5–38 μm set shows a
2 substantial variability in chemical composition, but no distinct differences between the samples
3 within the four localities. The 0.5–2.5 μm (fine) subsets of the three samples (S7, S8, and S9) are
4 different from the others in their higher Fe-rich (goethite, hematite) and carbon (carbonates)
5 components, and corresponding smaller amounts of clay (Fig. 6). This can be ascribed to a local
6 difference in the mineralogical composition of the undifferentiated source rocks (Edgell, 2006), as
7 well as weathering conditions.

8 The size and shapes of the thirteen < 38 μm sieved samples are given in Appendix A, Tables A1
9 and A2, with the average size distributions graphically displayed in Fig. 7. For individual samples,
10 the particle sizes are approximately log normally distributed (skewness 2.3–5.5), often showing a
11 slight bimodality, with a small maximum (approx. 12 μm) on the high end of the distributions. The
12 latter can be ascribed to harder, larger silt size particles of quartz and feldspars. The greatest
13 number of particles are tightly clustered about their mean diameters, resulting in high but variable
14 kurtosis values (4.6–44.0). The geometric mean diameters for the particles lie in the small range
15 of 2.1–3.7 μm , implying similar mineralogy and hardness. The mean aspect ratios of the particles
16 also fall in a tight range of 1.40–1.48, with a mean value of 1.43.

17 **5. Summary and Conclusions**

18 The impact of soil dust from natural and anthropogenic sources on climate and air quality has been
19 recognized on a global scale (Sokolik and Toon, 1996; Tegen and Fung, 1995). However, the
20 regional fine-scale processes of mineral dust emissions and their effect on the environmental
21 processes and human health are poorly quantified in the study region because the spatial
22 distribution of detailed mineralogical, physical and chemical properties of the surface soils at
23 coastal dust source regions (“hot-spots”) were previously not available.

24 The application of a range of techniques for the analysis of properties of soil samples allows for a
25 better understanding of mineral dust. However, the different analytical methods often provide
26 different results, as seen by comparing the XRD, electron microscopy and chemistry of the soils.
27 In this study, the results from the XRD analysis gives a quartz percentage of between about 19 and
28 44 % and sheet silicates (clays, micas) of between 3 and about 8%. In contrast, the single particle
29 analysis by CCSEM gives a quartz fraction of only up to about 10%, whereas the sheet silicates

1 always have the largest mineral percentage, of up to about 72%. This can lead to ambiguity in the
2 interpretation of the mineralogical composition of the samples. This is evident even where the
3 mineral composition is investigated for the same size range, i.e. < 38 µm particle diameter. Biases
4 in XRD results can be related to the presence of partly amorphous sheet silicates with poor
5 crystallization (Leinen et al., 1994; Formenti et al., 2011; Kandler et al., 2009; Engelbrecht et al.,
6 2016) and a subsequent overestimation of the quartz fractions. Knowing the answers to such
7 questions would be necessary for properly using the data to constrain or evaluate simulations with
8 dust models. Similarly, the individual particle analysis by CCSEM provides an overestimation of
9 the clay fraction which can be attributed to surface coatings on the quartz and its underestimation
10 (Engelbrecht et al., 2009a, b; Engelbrecht et al., 2016). What is of importance when considering
11 the application of these results in models, health studies, and remote sensing, is not only the
12 mineralogical composition of the dust, but also their mineralogical interrelationships such as
13 mineral clusters, mineral coatings, and intergrowths.

14 From satellite images we identified four Red Sea coastal areas from which dust was frequently
15 emitted (Jiang et al., 2009; Kalenderski et al., 2013). The thirteen soil grab samples were collected
16 from these areas for analysis and their mineralogy, chemical composition and particle size
17 distributions were studied. We found that the Red Sea coastal samples collected in this study
18 contain major components of quartz and feldspar (plagioclase, orthoclase), as well as lesser but
19 variable amounts of amphibole (hornblende), pyroxene (aegerine-augite), carbonate (calcite,
20 dolomite), clays (illite, palygorskite, kaolinite, smectite), and micas (muscovite, biotite), with
21 traces of gypsum, halite, chlorite, epidote and oxides. The range of identified minerals is ascribed
22 to the variety of igneous and metamorphic provenance rocks along the escarpment to the east of
23 the Red Sea coastal plain (Edgell, 2006). Similarly high fractions of quartz and feldspars were
24 reported for Kuwait (Engelbrecht et al., 2009b) and to a lesser extent for Tallil, Tikrit and Taji in
25 Iraq. The samples from the Red Sea coastal region of Saudi Arabia differ substantially from those
26 from Afghanistan, Qatar, UAE, Iraq and Kuwait in that they contain substantially less calcite. They
27 also contain much less dolomite than the sample from Al Asad in Iraq. These deviations in
28 composition could be ascribed to differences in provenance and geology. The coastal plain is
29 bounded by the Red Sea in the west, with the mountains of Midyan, Ash Shifa and Asir forming
30 an escarpment to the east and the provenance for water borne sediments to the wadis along the
31 coastal plain. Since the igneous and metamorphic source rocks are composed of a wide range of

Commented [JE3]: The date was corrected from 2008 to 2011

1 minerals including quartz, feldspars, amphiboles, pyroxenes, and micas, it can be assumed that the
2 partially weathered sediments transported to the coastal plain during flash floods will contain
3 similar minerals, which can in turn be suspended as mineral dust. In contrast the samples collected
4 in Kuwait, Iraq and Afghanistan are from extensive flat lying areas, and contain minerals such as
5 quartz, calcite, and dolomite from local sedimentary rocks.

6 Djibouti lies along the African Rift Valley along the west coast of the Gulf of Aden and close to
7 igneous and metamorphic rock formations of the Nubian Plate, separated from the petrographically
8 similar Arabian Plate by the Red Sea, both regions containing rock formations with substantial
9 amounts of pyroxene, amphibole, and plagioclase. This at least in part explains the similarity of
10 soils and dust at Djibouti to those along the coastal plain of Saudi Arabia, The mineralogical
11 content of the soils was found to be closely related to the regional geology.

12 Particle size analysis on the sampled soils showed them to contain too much sand and too little silt
13 to be considered major globally important sources of airborne dust, compared to renowned global
14 sources such as the Bodélé Depression, and silt covered regions of northwest U.S.A. (Engelbrecht
15 et al., 2012;Engelbrecht and Moosmüller, 2014). The low silt content in the investigated samples
16 suggests that the dust plume generated from the Red Sea coastal region is enriched by the coarse
17 dust fraction that deposits quickly. As seen from atmospheric observations, the coastal region is
18 the origin of frequent dust plumes over the Red Sea, probably due to frequent strong wind gusts.
19 These mostly coarse dusts could not be transported the vast distances to the Red Sea and directly
20 deposited there, affecting marine life. Our analysis revealed that the samples contain compounds
21 of nitrogen, phosphorus and iron, that are essential nutrients to marine life (Guerzoni et al.,
22 1997;Migon et al., 2001). The integration of analytical information on dust mineralogy and
23 mineralogical interrelationships, chemistry, and physical properties of soils provides a better
24 understanding of their potential impact on the communities living along the Red Sea (Edgell,
25 2006;UCAR/NCAR, 2003;Washington et al., 2003). The results from this study can also provide
26 improvements to the input of climate forecasting and dust emission models. The thirteen chemical
27 source profiles will complement those of soil samples collected in other regions of the Middle East
28 (Engelbrecht et al., 2009b), in source attribution studies.

1 Analytical methods developed in this phase of the dust program will be applied for analysis of dust
2 samples deposited from the atmosphere for aerosol characterization studies in the Red Sea coastal
3 region. These will allow further assessing the impact of elevated dust concentrations on regional
4 climate, marine ecology, air quality, and health.

5 **Data Availability**

6 The mineralogical and chemical data from this study are available upon request from Georgiy
7 Stenchikov (Georgiy.Stenchikov@kaust.edu.sa).

8 **Author Contributions**

9 Georgiy Stenchikov formulated the problem, designed the research project, and supported
10 experimental activities; Johann Engelbrecht advised on aerosol analysis and instrumentation;
11 Weichun Tao defined the dust source areas using satellite observations; Jish Prakash conducted
12 measurements, analysed and combined results; Tahir Yapici and Bashir Warsama helped with
13 instrumentation in the Kaust Core Lab. Prakash, Engelbrecht, and Stenchikov wrote different parts
14 of the paper.

15 **Acknowledgements**

16 This research, including the chemical and mineralogical analysis is supported by internal funding
17 from the King Abdullah University of Science and Technology (KAUST). For chemical analyses,
18 this research used the resources of the KAUST core lab. We acknowledge the contribution from
19 the collaborating laboratories of the RJ Lee Group and Desert Research Institute.

20

1 References

- 2 Aba-Husayn, M. M., Dixon, J. B., and Lee, S. Y.: Mineralogy of Saudi Arabian Soils:
3 Southwestern Region, *Soil Sci. Soc. Am. J.*, 44, 643-649,
4 10.2136/sssaj1980.03615995004400030043x, 1980.
- 5 Acosta, F., Ngugi, D. K., and Stingl, U.: Diversity of picoeukaryotes at an oligotrophic site off
6 the Northeastern Red Sea Coast, *Aquat. Biosyst.*, 9, 10.1186/2046-9063-9-16, 2013.
- 7 Al-Farraj, A. S.: The mineralogy of clay fractions in the soils of the southern region of Jazan,
8 Saudi Arabia, *J. Agron.*, 7, 115-126, 2008.
- 9 Bennett, C. M., McKendry, I. G., Kelly, S., Denike, K., and Koch, T.: Impact of the 1998 Gobi
10 dust event on hospital admissions in the Lower Fraser Valley, British Columbia, *Sci. Total*
11 *Environ.*, 366, 918-925, doi: 10.1016/j.scitotenv.2005.12.025, 2006.
- 12 Bennion, P., Hubbard, R., O'Hara, S., Wiggs, G., Wegerdt, J., Lewis, S., Small, I., van der Meer,
13 J., and Upshur, R.: The impact of airborne dust on respiratory health in children living in the
14 Aral Sea region, *Int. J. Epidemiol.*, 36, doi: 1103-1110, 10.1093/ije/dym195, 2007.
- 15 Brindley, H., Osipov, S., Bantges, R., Smirnov, A., Banks, J., Levy, R., Jish Prakash, P., and
16 Stenchikov, G.: An assessment of the quality of aerosol retrievals over the Red Sea and
17 evaluation of the climatological cloud-free dust direct radiative effect in the region, *J.*
18 *Geophys. Res.: Atmos.*, 120, doi: 2015JD023282, 10.1002/2015JD023282, 2015.
- 19 Bristow, C. S., Hudson-Edwards, K. A., and Chappell, A.: Fertilizing the Amazon and equatorial
20 Atlantic with West African dust, *Geophysical Research Letter*, 37, L14807,
21 doi:10.1029/2010GL043486, 2010.
- 22 Buseck, P. R., Jacob, D. J., Pósfai, M., Li, J., and Anderson, J. R.: Minerals in the air: An
23 environmental perspective, *International Geology Review*, Symposium, Stanford, California,
24 1999.
- 25 Caquineau, S., Magonthier, M.-C., Gaudichet, A., and Gomes, L.: An improved procedure for
26 the X-ray diffraction analysis of low-mass atmospheric dust samples, *Eur. J. Mineral.*, 9, 157-
27 166, 1997.
- 28 Chung, F. H.: Quantitative interpretation of X-ray diffraction patterns of mixtures. I. Matrix-
29 flushing method for quantitative multicomponent analysis, *J. Appl. Crystallogr.*, 7, 519-525,
30 doi:10.1107/S0021889874010375 1974.
- 31 De Longueville, F., Hountondji, Y. C., Henry, S., and Ozer, P.: What do we know about effects
32 of desert dust on air quality and human health in West Africa compared to other regions?, *Sci.*
33 *Total Environ.*, 409, 1-8, 2010.
- 34 Edgell, H. S.: *Arabian Deserts. Nature, Origin and Evolution*, Springer, Dordrecht, Netherlands,
35 592 pp., 2006.
- 36 Engelbrecht, J. P., McDonald, E. V., Gillies, J. A., Jayanty, R. K. M., Casuccio, G., and Gertler,
37 A. W.: Characterizing mineral dusts and other aerosols from the Middle East – Part 1:
38 Ambient sampling, *Inhalation Toxicol.*, 21, 297-326, 2009a.

- 1 Engelbrecht, J. P., McDonald, E. V., Gillies, J. A., Jayanty, R. K. M., Casuccio, G., and Gertler,
2 A. W.: Characterizing mineral dusts and other aerosols from the Middle East – Part 2: Grab
3 samples and re-suspensions, *Inhalation Toxicol.*, 21, 327-336, 2009b.
- 4 Engelbrecht, J. P., Gillies, J. A., Etyemezian, V., Kuhns, H., Baker, S. E., Zhu, D., Nikolich, G.,
5 and Kohl, S. D.: Controls on mineral dust emissions at four arid locations in the western USA,
6 *Aeolian Res.*, 6, 41-54, 2012.
- 7 Engelbrecht, J. P., and Moosmüller, H.: Mobile Aerosol Monitoring System for Department of
8 Defense - Continuous Aerosol and Aerosol Optics Measurement in Theater, U.S. Army
9 Medical Research and Materiel Command, Fort Detrick, Maryland Report W81XWH-11-2-
10 0220, 1-229, 2014.
- 11 Engelbrecht, J. P., Moosmüller, H., Pincock, S., Jayanty, R. M., Lersch, T., and Casuccio, G.:
12 Technical Note: Mineralogical, chemical, morphological, and optical interrelationships of
13 mineral dust re-suspensions, *Atmospheric Chemistry and Physics*, doi: 10.5194/acp-16-
14 10809-2016, 2016.
- 15 Esteve, V., Rius, J., Ochando, L. E., and Amigó, J. M.: Quantitative x-ray diffraction phase
16 analysis of coarse airborne particulate collected by cascade impactor sampling, *Atmos. Env.*,
17 31, 3963-3967, doi:10.1016/S1352-2310(97)00257-4, 1997.
- 18 Formenti, P., Rajot, J. L., Desboeufs, K., Said, F., Grand, N., Chevaillier, S., and Schmechtig, C.:
19 Airborne observations of mineral dust over western Africa in the summer Monsoon season:
20 spatial and vertical variability of physico-chemical and optical properties, *Atmospheric
21 Chemistry and Physics*, 11, 6387–6410, doi: 10.5194/acp-11-6387-2011, 2011.
- 22 Fryrear, D. W.: Long-term effect of erosion and cropping on soil productivity, *Spec. Pap. - Geol.
23 Soc. Am.*, 186, 253-260, doi: 10.1130/SPE186-p253, 1981.
- 24 Gee, G. W., and Or, D.: Particle-size analysis, in: *Methods of Soil Analysis: Part 4–Physical
25 Methods*, No. 5, edited by: Dane, J. H., and Topp, G. C., Soil Science Society of America,
26 Madison, WI., 255-293, 2002.
- 27 Gillette, D. A., and Walker, T. R.: Characteristics of airborne particles produced by wind erosion
28 of sandy soil, *High Plains of West Texas, Soil Sci.*, 123, 97-110, 1977.
- 29 Goudie, A. S., and Middleton, N.J.: *Desert Dust in the Global System*, Springer, Germany, 287
30 pp., 2006.
- 31 Grainger, D.: *The Geological Evolution of Saudi Arabia, a Voyage through Space and Time*
32 *Saudi Geological Survey, Jeddah, Saudi Arabia, ISBNs 9781905755073, 1905755074, 264
33 pp., 2007.*
- 34 Greely, R., and Iversen, J. D.: *Wind as a geological process on Earth, Mars, and Venus*,
35 Cambridge University Press, Cambridge, 333 pp., 1985.
- 36 Grell, G., Peckham, S. E., Schmitz, R., A., M. S., Frost, G., Skamarock, W. C., and Eder, B.:
37 Fully coupled "online" chemistry within the WRF Model, *Atmos. Env.*, 39, 6957-6975, 2005.
- 38 Guerzoni, S., Molinaroli, E., and Chester, R.: Saharan dust inputs to the western Mediterranean
39 Sea: depositional patterns, geochemistry and sedimentological implications, *Deep Sea Res.*,
40 Part II, 44, 631–654, 1997.

- 1 Hagen, L. J., and Woodruff, N. P.: Air pollution from dust storms in the Great Plains, *Atmos.*
2 *Env.*, 7, 323-332, 1973.
- 3 Haywood, J., and Boucher, O.: Estimates of the direct and indirect radiative forcing due to
4 tropospheric aerosols: A review, *Rev. Geophys.*, 38, 513-543, doi: 10.1029/1999RG000078,
5 2000.
- 6 Hsu, N. C., Tsay, S. C., King, M. D., and Herman, J. R.: Aerosol properties over bright-
7 reflecting source regions, *IEEE Trans. Geosci.*, 42, 557-569, 2004.
- 8 Huang, J., Minnis, P., Lin, B., Wang, T., Yi, Y., Hu, Y., Sun-Mack, S., and Ayers, K.: Possible
9 influences of Asian dust aerosols on cloud properties and radiative forcing observed from
10 MODIS and CERES, *Geophys. Res. Lett.*, 33, L06824, doi: 10.1029/2005GL024724, 2006.
- 11 Huang, J., Wang, T., Wang, W., Li, Z., and Yan, H.: Climate effects of dust aerosols over East
12 Asian arid and semiarid regions, *J. Geophys. Res.: Atmos.*, 119, 2014JD021796, doi:
13 10.1002/2014JD021796, 2014.
- 14 Jiang, H., Farrar, J. T., Beardsley, R. C., Chen, R., and Chen, C.: Zonal surface wind jets across
15 the Red Sea due to mountain gap forcing along both sides of the Red Sea, *Geophys. Res.*
16 *Lett.*, 36, L19605, doi: 10.1029/2009GL040008, 2009.
- 17 Jickells, T. D., An, Z. S., Andersen, K. K., Baker, A. R., Bergametti, G., Brooks, N., Cao, J. J.,
18 Boyd, P. W., Duce, R. A., Hunter, K. A., Kawahata, H., Kubilay, N., laRoche, J., Liss, P. S.,
19 Mahowald, N., Prospero, J. M., Ridgwell, A. J., Tegen, I., and Torres, R.: Global iron
20 connections between desert dust, ocean biogeochemistry, and climate, *Science*, 308, 67-71,
21 2005.
- 22 Kalenderski, S., Stenichkov, G., and Zhao, C.: Modeling a typical winter-time dust event over
23 the Arabian Peninsula and the Red Sea, *Atmos. Chem. Phys.*, 13, 1999-2014, 10.5194/acp-13-
24 1999-2013, 2013.
- 25 Kandler, K., Schütz, L., Deutscher, C., Ebert, M., Hofmann, H., Jäckel, S., Jaenicke, R.,
26 Knippertz, P., Lieke, K., Massling, A., Petzold, A., Schladitz, A., Weinzierl, B.,
27 Wiedensohler, A., Zorn, S., and Weinbruch, S.: Size distribution, mass concentration,
28 chemical and mineralogical composition and derived optical parameters of the boundary layer
29 aerosol at Tinfou, Morocco, during SAMUM 2006, *Tellus*, 61B, 32-50, 2009.
- 30 Kerr, P. F.: *Optical Mineralogy*, 3rd ed., McGraw-Hill Book Company, Inc., USA, 442 pp.,
31 1959.
- 32 Kok, J. F.: A scaling theory for the size distribution of emitted dust aerosols suggests climate
33 models underestimate the size of the global dust cycle, *Proc. Natl. Acad. Sci.*, 108, 1016–
34 1021, 2011a.
- 35 Kok, J. F.: Does the size distribution of mineral dust aerosols depend on the wind speed at
36 emission?, *Atmos. Chem. Phys.*, 11, 10149–10156, 2011b.
- 37 Kumar, R., Barth, M. C., Pfister, G. G., Naja, M., and Brasseur, G. P.: WRF-Chem simulations
38 of a typical pre-monsoon dust storm in northern India: influences on aerosol optical properties
39 and radiation budget, *Atmos. Chem. Phys.*, 14, 2431-2446, doi: 10.5194/acp-14-2431-2014,
40 2014.

1 Leinen, M., Prospero, J. M., Arnold, E., and Blank, M.: Mineralogy of aeolian dust reaching the
2 North Pacific Ocean 1. Sampling and analysis, *Journal of Geophysical Research*, 99, 21,017-
3 021,023, 1994.

4 Mahowald, N., S. Engelstaedter, C. Luo, A. Sealy, P. Artaxo, C. Benitez-Nelson, S. Bonnet, Y.
5 Chen, P.Y. Chuang, D.D. Cohen, F. Dulac, B. Herut, A.M. Johansen, N. Kubilay, R. Losno,
6 W. Maenhaut, A. Paytan, J.M. Prospero, L.M. Shank, and R.L. Siefert: Atmospheric iron
7 deposition: Global distribution, variability and human perturbations, *Ann. Rev. Marine Sci.*,
8 1, 245-278, 2009.

9 Marticorena, B., and Bergametti, G.: Modeling the atmospheric dust cycle: 1. Design of a soil-
10 derived dust emission scheme, *J. Geophys. Res.: Atmos.*, 100, 16415-16430,
11 10.1029/95JD00690, 1995.

12 Marticorena, B.: Dust production mechanisms, in: *Mineral Dust: A Key Player in the Earth*
13 *System*, edited by: Knippertz, P., and Stuut, J.-B. W., Springer Science+Business Media,
14 Dordrecht, 93-120, 2014.

15 Menéndez, I., Pérez-Chacón, E., Mangas, J., Tauler, E., Engelbrecht, J. P., Derbyshire, E., Cana,
16 L., and Alonso, I.: Dust deposits on La Graciosa Island (Canary Islands, Spain): Texture,
17 mineralogy and a case study of recent dust plume transport, *Catena*, 117, 133-144, 2014.

18 Menut, L., Pérez, C., Haustein, K., Bessagnet, B., Prigent, C., and Alfaro, S.: Impact of surface
19 roughness and soil texture on mineral dust emission fluxes modeling, *J. Geophys. Res.:*
20 *Atmos.*, 118, 6505-6520, doi: 10.1002/jgrd.50313, 2013.

21 Migon, C., Sandroni, V., and Béthoux, J. P.: Atmospheric input of anthropogenic phosphorus to
22 the northwest Mediterranean under oligotrophic conditions, *Mar. Environ. Res.*, 7, 1-14.,
23 2001.

24 Moosmüller, H., Engelbrecht, J. P., Skiba, M., Frey, G., Chakrabarty, R. K., and Arnott, W. P.:
25 Single scattering albedo of fine mineral dust aerosols controlled by iron concentration, *J.*
26 *Geophys. Res.*, 117, D11210, doi:10.1029/2011JD016909, 10.1029/2011JD016909, 2012.

27 Muhs, D. R., Prospero, J. M., Baddock, M. C., and Gill, T. E.: Identifying sources of aeolian
28 mineral dust: Present and past, in: *Mineral Dust, A Key Player in the Earth System*, edited by:
29 Knippertz, P., and Stuut, J.-B. W., Springer Science+Business Media, Dordrecht, 51-74,
30 2014.

31 Nickovic, S., Vukovic, A., Vujadinovic, M., Djurdjevic, V., and Pejanovic, G.: Technical Note:
32 High-resolution mineralogical database of dust-productive soils for atmospheric dust
33 modeling, *Atmos. Chem. Phys.*, 12, 845–855, 2012.

34 Nihlen, T., and Lund, S. O.: Influence of Aeolian Dust on Soil Formation in the Aegean Area, *Z.*
35 *Geomorphol.*, 393, 341-361, 1995.

36 Oleson, K. W., Lawrence, D. M., Bonan, G. B., Flanner, M. G., Kluzek, E., Lawrence, P. J.,
37 Levis, S., Swenson, S. C., Thornton, P. E., Dai, A., Decker, M., Dickinson, R., Feddema, J.,
38 Heald, C. L., Hoffman, F., Lamarque, J., Mahowald, N., Niu, G., Qian, T., Randerson, J.,
39 Running, S., Sakaguchi, K., Slater, A., Stockli, R., Wang, A., Yang, Z., Zeng, X., and Zeng,
40 X.: Technical Description of version 4.0 of the Community Land Model (CLM). , NCAR
41 Technical Note NCAR/TN-478+STR, 2010.

- 1 Osipov, S., Stenchikov, G., Brindley, H., and Banks, J.: Diurnal cycle of the dust instantaneous
2 direct radiative forcing over the Arabian Peninsula, *Atmos. Chem. Phys.*, 15, 9537-9553, doi:
3 10.5194/acp-15-9537-2015, 2015.
- 4 Perlwitz, J. P., Pérez García-Pando, C., and Miller, R. L.: Predicting the mineral composition of
5 dust aerosols – Part 2: Model evaluation and identification of key processes with
6 observations, *Atmos. Chem. Phys.*, 15, 11629-11652, doi: 10.5194/acp-15-11629-2015,
7 2015a.
- 8 Perlwitz, J. P., Pérez García-Pando, C., and Miller, R. L.: Predicting the mineral composition of
9 dust aerosols – Part 1: Representing key processes, *Atmos. Chem. Phys.*, 15, 11593-11627,
10 doi: 10.5194/acp-15-11593-2015, 2015b.
- 11 Prakash, J. P., Stenchikov, G., Kalenderski, S., Osipov, S., and Bangalath, H.: The impact of dust
12 storms on the Arabian Peninsula and the Red Sea, *Atmos. Chem. Phys.*, 15, 199-222, doi:
13 10.5194/acp-15-199-2015, 2015.
- 14 Prospero, J. M., Ginoux, P., Torres, O., Nicholson, S. E., and Gill, T. E.: Environmental
15 characterization of global sources of atmospheric soil dust identified with the NIMBUS 7
16 total ozone mapping spectrometer (TOMS) absorbing aerosol product, *Rev. Geophys.*, 40, 31,
17 doi: 10.1029/2000RG000095, 2002.
- 18 Roquin, C., Freyssinet, P., Zeegers, H., and Tardy, Y.: Element distribution patterns in laterites
19 of southern Mali: Consequence for geochemical prospecting and mineral exploration, *Applied
20 Geochemistry*, 5, 303-315, 1990.
- 21 Rietveld, H. M.: A profile refinement method for nuclear and magnetic structures, *J. Appl.
22 Crystallogr.*, 2, 65-71, doi: 10.1107/S0021889869006558, 1969.
- 23 Scheuven, D., and Kandler, K.: On composition, morphology, and size distribution of airborne
24 mineral dust, in: *Mineral Dust, a Key Player in the Earth System*, edited by: Knippertz, P.,
25 and Stuut, J.-B. W., Springer Science+Business Media, Dordrecht, 15-49, 2014.
- 26 Shadfai, H., Mashhady, A., Eter, A., and Hussen, A. A.: Mineral composition of selected soils in
27 Saudi Arabia, *J. Plant Nutr. Soil Sci.*, 147, 657-668, doi: 10.1002/jpln.19841470603, 1984.
- 28 Sokolik, I. N., and Toon, O. B.: Direct radiative forcing by anthropogenic airborne mineral
29 aerosols, *Nature*, 381, 681-683, 1996.
- 30 Sokolik, I. N., and Toon, O. B.: Incorporation of mineralogical composition into models of the
31 radiative properties of mineral aerosol from UV to IR wavelengths, *J. Geophys. Res.: Atmos.*,
32 104, 9423-9444, doi: 10.1029/1998JD200048, 1999.
- 33 Sturges, W. T., Harrison, R. M., and Barrie, L. A.: Semi-quantitative X-ray diffraction analysis
34 of size fractionated atmospheric particles, *Atmos. Env.*, 23, 1083-1098, 1989.
- 35 Tanaka, T. Y., and Chiba, M.: A numerical study of the contributions of dust source regions to
36 the global dust budget, *Global Planet. Change*, 52, 88-104, 2006.
- 37 Tegen, I., and Fung, I.: Contribution to the atmospheric mineral aerosol load from land surface
38 modification, *J. Geophys. Res.*, 100, 18707-18726, 1995.
- 39 Twomey, S. A., Piepgrass, M., and Wolfe, T. L.: An assessment of the impact of pollution on
40 global cloud albedo, *Tellus B*, 36, doi: 10.3402/tellusb.v36i5.14916, 2011.

1 UCAR/NCAR: Forecasting Dust Storms, National Center for Atmospheric Research, Boulder,
2 National Center for Atmospheric Research, Boulder, 1-67, 2003.

3 Viani, B. E., A. S. Al-Mashhady, and Dixon, J. B.: Mineralogy of Saudi Arabian Soils: Central
4 Alluvial Basins, *Soil Sci. Soc. Am. J.*, 47, 149-157, doi:
5 10.2136/sssaj1983.03615995004700010030x, 1983.

6 Wang, W., Huang, J., Minnis, P., Hu, Y., Li, J., Huang, Z., Ayers, J. K., and Wang, T.: Dusty
7 cloud properties and radiative forcing over dust source and downwind regions derived from
8 A-Train data during the Pacific Dust Experiment, *J. Geophys. Res.: Atmos.*, 115, D00H35,
9 doi: 10.1029/2010JD014109, 2010.

10 Wang, Z., Ueda, H., and Huang, M.: A deflation module for use in modeling long-range
11 transport of yellow sand over East Asia, *J. Geophys. Res.: Atmos.*, 105, 26947-26959, doi:
12 10.1029/2000JD900370, 2000.

13 Washington, R., Todd, M. C., Middleton, N. J., and Goudie, A. S.: Dust-storm source areas
14 determined by the total ozone monitoring spectrometer and surface observations, *Ann. Assoc.
15 Am. Geogr.*, 93, 297-313, 2003.

16 Washington, R., and Todd, M. C.: Atmospheric controls on mineral dust emission from the
17 Bodélé depression, Chad: The role of the low level jet, *Geophys. Res. Lett.*, 32, L17701,
18 doi:10.1029/2005GL023597, 2005.

19 Webb, N. P., and Strong, C. L.: Soil erodibility dynamics and its representation for wind erosion
20 and dust emission models, *Aeolian Res.*, 3, 165-179, doi: 10.1016/j.aeolia.2011.03.002, 2011.

21 Weese, C. B., and Abraham, J. H.: Potential health implications associated with particulate
22 matter exposure in deployed settings in Southwest Asia, *Inhalation Toxicol.*, 21, 291-296,
23 2009.

24 Zender, C. S., Huisheng, B., and David, N.: Mineral Dust Entrainment and Deposition (DEAD)
25 model: Description and 1990s dust climatology, *J. Geophys. Res.: Atmos.*, 108, 2003.

26
27

Commented [JE4]:

1
2
3

Table1. Localities of soil sampling sites along the Red Sea coastal plain.

Site	Proximity	Latitude	Longitude	Elevation (m)
S1	SE of Al Nasaif	23.3322° N	38.9481° E	94
S2	SE of Al Nasaif	23.2961° N	38.9385° E	68
S3	SE of Al Nasaif	23.2920° N	38.9100° E	46
S4	E of Ar Rayis	23.5876° N	38.9243° E	128
S5	E of Ar Rayis	23.5746° N	38.9213° E	118
S6	E of Ar Rayis	23.5656° N	38.9193° E	115
S7	N of Yanbu	24.3334° N	38.0205° E	113
S8	N of Yanbu	24.3239° N	38.0254° E	60
S9	N of Yanbu	24.3195° N	38.0245° E	56
S10	SW of Mecca	21.3197° N	39.5763° E	128
S11	SW of Mecca	21.3232° N	39.5711° E	124
S12	SW of Mecca	21.3211° N	39.5593° E	133
S13	SW of Mecca	21.3253° N	39.5508° E	118

4
5

1

2

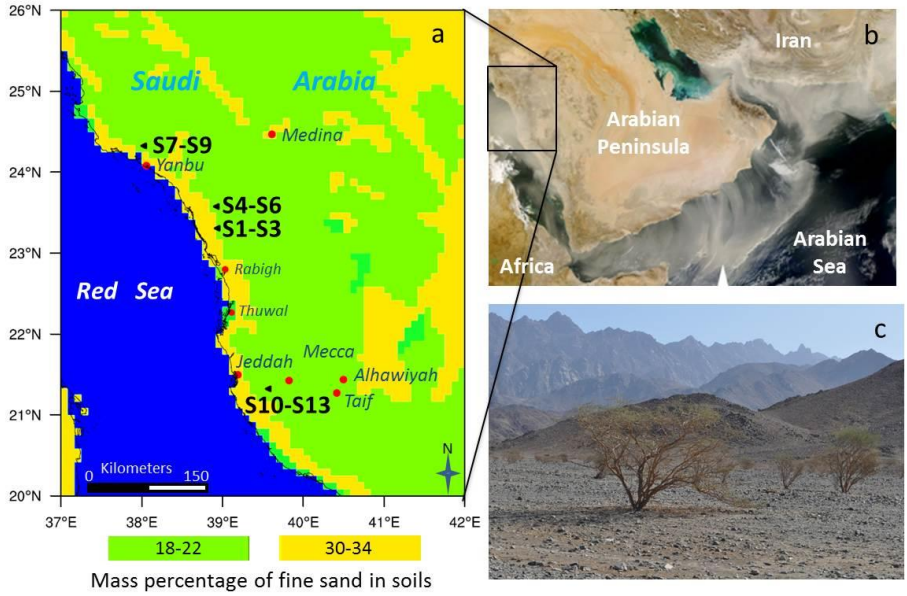
3 **Table 2.** The volume particle size fraction (%) of the < 600 μm sieved soil samples.

Sample	Sand (600–62.5 μm)	Silt (62.5–2 μm)	Clay (< 2 μm)
S1	78.0	19.2	2.8
S2	77.2	20.5	2.3
S3	93.3	5.7	1.0
S4	96.3	3.0	0.7
S5	88.4	10.0	1.7
S6	88.5	9.8	1.6
S7	94.3	5.2	0.5
S8	93.5	6.0	0.5
S9	87.1	12.1	0.9
S10	87.8	10.6	1.6
S11	86.6	11.4	1.9
S12	91.1	7.6	1.2
S13	92.7	6.1	1.2

4

5

1
2



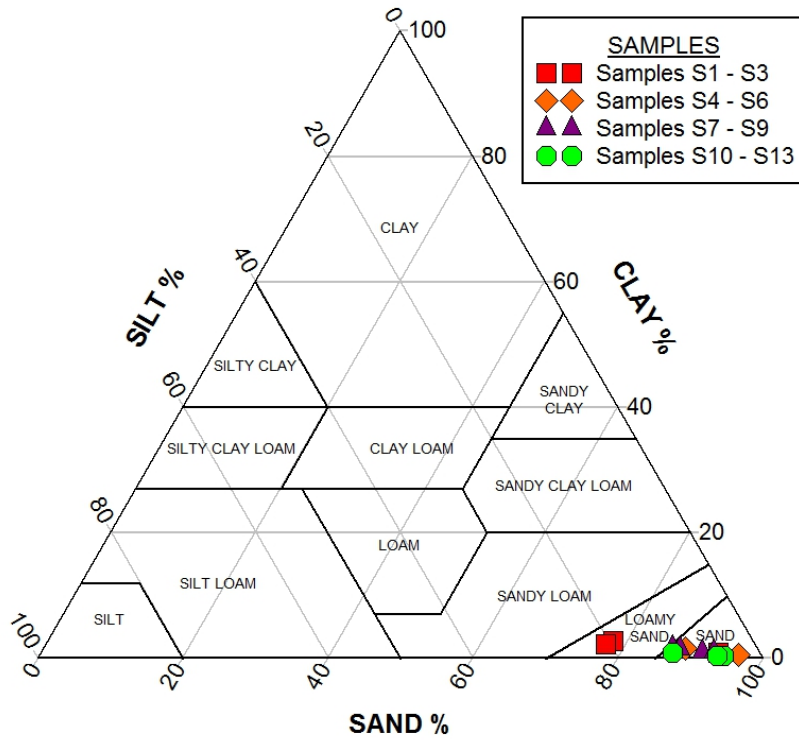
3

4 **Fig. 1 (a)**, Map showing the mass percentage of fine sand in soils, based on STATSGO-FAO soil
5 texture data (Nickovic et al., 2012; Menut et al., 2013), in the Arabian Peninsula, as well as the four
6 localities and thirteen (S1–S13) sampling sites. **(b)** Modis satellite image of dust storm over the
7 Arabian Peninsula captured on February 22, 2008 (NASA Modis web site). **(c)** Sampling site S1
8 showing the typical acacia trees growing along the wadi in the foreground, with the Hejaz
9 mountain range and escarpment in the distance.

10

11

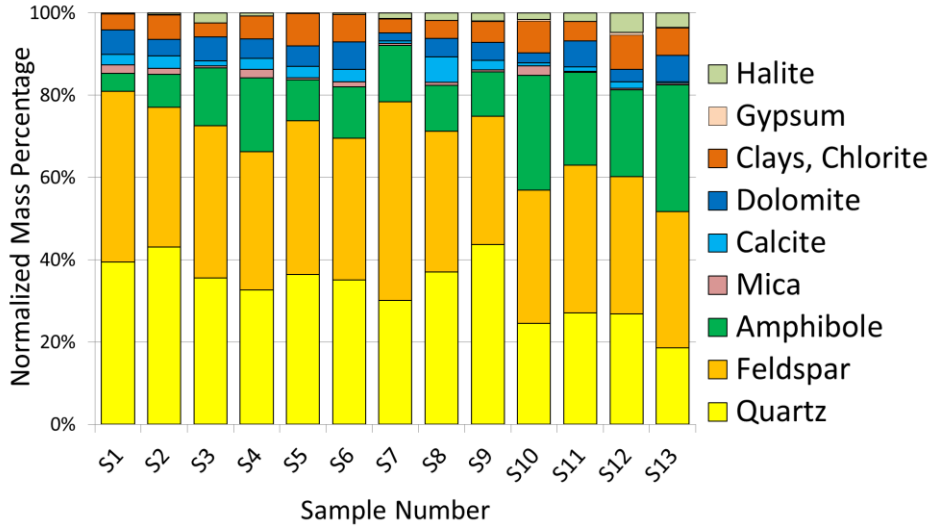
1
2



3
4
5
6
7
8

Fig 2. US Department of Agriculture (USDA) soil texture triangle showing the grain size plot of the thirteen samples collected for this study. Volume size-class fractions grouped as clay (< 2 μm), silt (> 2, < 62.5 μm) and sand (> 62.5, < 600 μm).

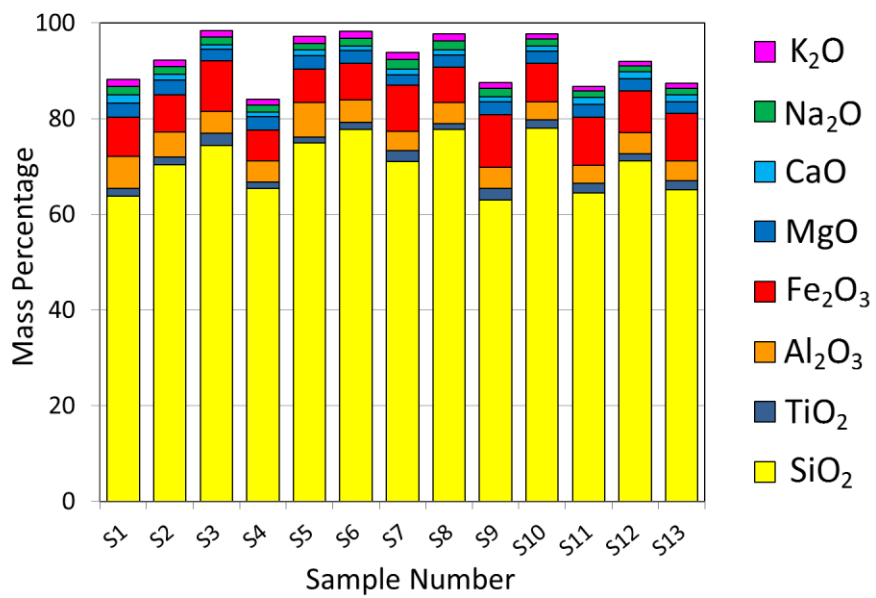
1
2



3
4
5
6
7

Fig 3. Normalized mineral compositions by percentage of mass of thirteen < 38 μm sieved soil samples collected at four localities along the Red Sea coastal area, as measured by XRD.

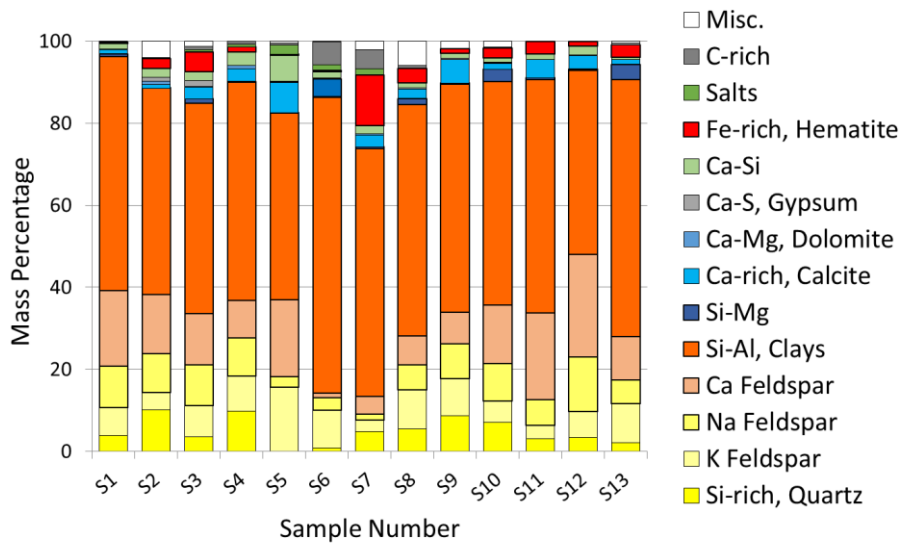
1
2



3
4
5
6
7

Fig. 4. Compositional plot showing major oxides percentages by mass from ICP-OES analysis of < 38 μm sieved soils.

1
2



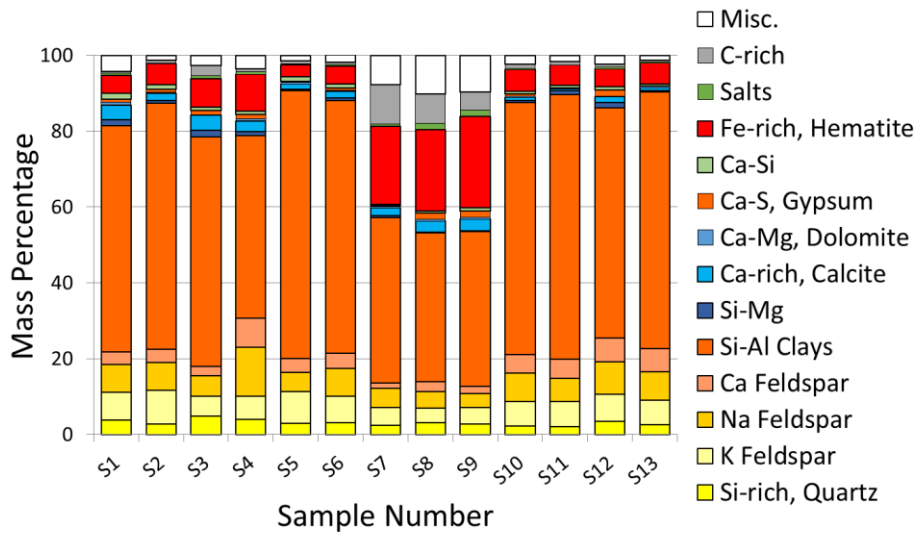
3

4 **Fig. 5.** CCSEM based individual particle analysis for the 0.5-38 μm chemical set, with the
5 chemical bins labeled as minerals, by normalized mass percentages.

6

7

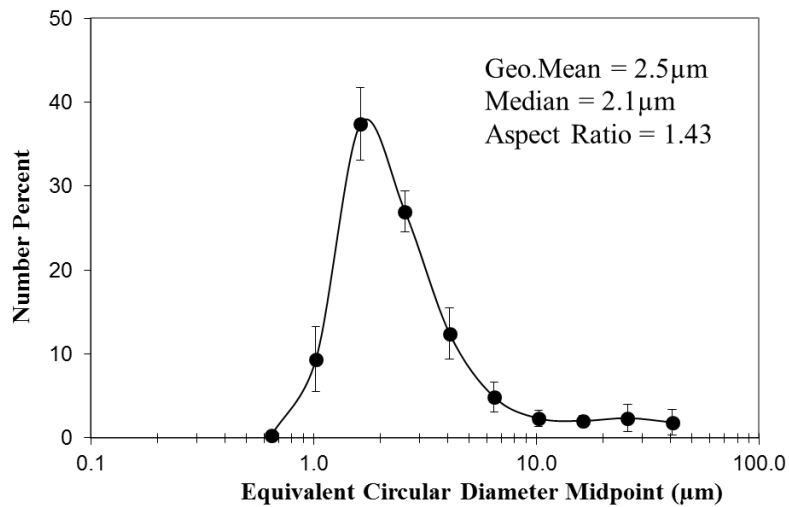
1
2



3
4
5
6
7

Fig. 6. CCSEM based individual particle analysis for 0.5-2.5 μm (fine) subset, with the chemical bins labeled as minerals, by normalized mass percentages.

1
2



3
4
5
6
7

Fig. 7. Average and standard deviations of particle sizes, as well as size and shape statistics for thirteen < 38 μm sieved samples, as measured by CCSEM.

1
2
3 **Appendix A**
4 **Table A1.** Major, minor and trace element compositions of grab samples, S1 to S3 collected near
5 Al Nasaif, and S4 to S6 collected near Ar Rayis, all along the Red Sea coastal region. Also
6 tabulated are elemental mass ratios, statistics of the individual particle sizes and morphology as
measured by CCSEM.

Sample #	S1		S2		S3		S4		S5		S6	
Major and minor elements as oxides (%)												
	Conc.	Unc.	Conc.	Unc.	Conc.	Unc.	Conc.	Unc.	Conc.	Unc.	Conc.	Unc.
SiO ₂	63.795 ± 3.190		70.302 ± 3.515		74.337 ± 3.717		65.436 ± 3.272		74.872 ± 3.744		77.668 ± 3.883	
TiO ₂	1.577 ± 0.079		1.700 ± 0.085		2.536 ± 0.127		1.300 ± 0.065		1.237 ± 0.062		1.511 ± 0.076	
Al ₂ O ₃	6.768 ± 0.338		5.195 ± 0.260		4.664 ± 0.233		4.367 ± 0.218		7.260 ± 0.363		4.710 ± 0.236	
Fe ₂ O ₃	8.195 ± 0.410		7.777 ± 0.389		10.497 ± 0.525		6.535 ± 0.327		6.936 ± 0.347		7.584 ± 0.379	
MnO	0.112 ± 0.006		0.119 ± 0.006		0.135 ± 0.007		0.109 ± 0.005		0.123 ± 0.006		0.144 ± 0.007	
MgO	2.903 ± 0.145		3.137 ± 0.157		2.478 ± 0.124		2.741 ± 0.137		2.824 ± 0.141		2.767 ± 0.138	
CaO	1.723 ± 0.086		1.200 ± 0.060		0.895 ± 0.045		0.900 ± 0.045		1.249 ± 0.062		0.909 ± 0.045	
Na ₂ O	1.695 ± 0.085		1.577 ± 0.079		1.657 ± 0.083		1.494 ± 0.075		1.248 ± 0.062		1.659 ± 0.083	
K ₂ O	1.473 ± 0.074		1.372 ± 0.069		1.269 ± 0.063		1.198 ± 0.060		1.579 ± 0.079		1.484 ± 0.074	
P ₂ O ₅	0.406 ± 0.048		0.353 ± 0.047		0.400 ± 0.048		0.364 ± 0.048		0.291 ± 0.046		0.403 ± 0.048	
Total	88.649		92.734		98.867		84.444		97.620		98.838	
Trace elements (ppm)												
Li	17 ± 1		21 ± 1		15 ± 1		19 ± 1		24 ± 1		22 ± 1	
V	183 ± 9		182 ± 9		242 ± 12		161 ± 8		166 ± 8		191 ± 10	
Cr	114 ± 6		103 ± 5		150 ± 8		83 ± 4		91 ± 5		98 ± 5	
Co	30 ± 1		27 ± 1		26 ± 1		29 ± 1		28 ± 1		29 ± 1	
Ni	55 ± 3		52 ± 3		46 ± 2		45 ± 2		48 ± 2		50 ± 3	
Cu	29 ± 1		33 ± 2		24 ± 1		42 ± 2		40 ± 2		42 ± 2	
Zn	39 ± 2		39 ± 2		40 ± 2		39 ± 2		47 ± 2		90 ± 5	
Sr	294 ± 16		333 ± 18		358 ± 19		288 ± 15		285 ± 15		306 ± 16	
Ba	318 ± 16		426 ± 21		342 ± 17		408 ± 20		502 ± 25		610 ± 30	
Water soluble ions (%)												
Mg ²⁺	0.046 ± 0.001		0.038 ± 0.001		0.027 ± 0.001		0.036 ± 0.001		0.044 ± 0.001		0.143 ± 0.004	
Ca ²⁺	0.171 ± 0.022		0.106 ± 0.014		0.071 ± 0.009		0.107 ± 0.014		0.162 ± 0.021		0.455 ± 0.058	
Na ⁺	0.024 ± 0.001		0.005 ± 0.001		0.007 ± 0.001		0.005 ± 0.001		0.008 ± 0.001		0.025 ± 0.003	
K ⁺	0.020 ± 0.002		0.010 ± 0.001		0.008 ± 0.001		0.011 ± 0.001		0.025 ± 0.002		0.037 ± 0.004	
Cl ⁻	0.092 ± 0.004		0.000 ± 0.001		0.000 ± 0.001		0.000 ± 0.001		0.040 ± 0.002		0.222 ± 0.010	
SO ₄ ²⁻	0.078 ± 0.001		0.031 ± 0.001		0.017 ± 0.001		0.126 ± 0.002		0.131 ± 0.002		0.466 ± 0.007	
PO ₄ ³⁻	0.002 ± 0.001		0.002 ± 0.001		0.000 ± 0.001		0.000 ± 0.001		0.002 ± 0.001		0.006 ± 0.004	
NO ₃ ⁻	0.018 ± 0.002		0.006 ± 0.001		0.011 ± 0.001		0.016 ± 0.002		0.019 ± 0.002		0.076 ± 0.007	
Mass ratios												
Si/Al	8.321		11.946		14.071		13.227		9.105		14.558	
Ca/Al	0.344		0.312		0.259		0.279		0.233		0.261	
Fe/Al	1.600		1.978		2.974		1.977		1.262		2.128	
Particle diameter from CCSEM measurements (approx. 2000 particles)(µm)												
Geom. Mean (µm)	2.81		2.12		3.50		2.24		2.53		2.35	
Arith. Mean (µm)	3.66		2.72		6.75		3.25		3.29		3.00	
Skewness	4.57		4.32		2.34		5.04		5.44		5.51	
Kurtosis	28.85		25.20		4.63		29.43		40.11		44.00	
Mean aspect ratio	1.41		1.42		1.48		1.45		1.41		1.41	

7
8

1
2
3 **Appendix A**
4 **Table A2.** Major, minor and trace element compositions of grab samples S7 to S9 collected near
5 Yanbu, and S10 to S13 near Mecca, all along the Red Sea coastal region. Also tabulated are
6 elemental mass ratios, statistics of the individual particle size and morphology as measured by
CCSEM.

Sample #	S7		S8		S9		S10		S11		S12		S13	
Major and minor elements as oxides (%)														
	Conc.	Unc.	Conc.	Unc.	Conc.	Unc.	Conc.	Unc.	Conc.	Unc.	Conc.	Unc.	Conc.	Unc.
SiO ₂	71.041 ± 3.552		77.76 ± 3.888		62.997 ± 3.150		78.006 ± 3.900		64.44 ± 3.222		71.091 ± 3.555		65.173 ± 3.259	
TiO ₂	2.246 ± 0.112		1.22 ± 0.061		2.401 ± 0.120		1.793 ± 0.090		2.09 ± 0.104		1.499 ± 0.075		1.786 ± 0.089	
Al ₂ O ₃	4.080 ± 0.204		4.33 ± 0.217		4.351 ± 0.218		3.697 ± 0.185		3.70 ± 0.185		4.516 ± 0.226		4.198 ± 0.210	
Fe ₂ O ₃	9.563 ± 0.478		7.43 ± 0.371		11.027 ± 0.551		7.997 ± 0.400		10.07 ± 0.504		8.604 ± 0.430		9.936 ± 0.497	
MnO	0.121 ± 0.006		0.10 ± 0.005		0.156 ± 0.008		0.126 ± 0.006		0.13 ± 0.007		0.115 ± 0.006		0.117 ± 0.006	
MgO	2.255 ± 0.113		2.53 ± 0.127		2.76 ± 0.138		2.549 ± 0.127		2.62 ± 0.131		2.556 ± 0.128		2.345 ± 0.117	
CaO	1.109 ± 0.055		1.02 ± 0.051		1.071 ± 0.054		1.064 ± 0.053		1.55 ± 0.077		1.547 ± 0.077		1.586 ± 0.079	
Na ₂ O	2.015 ± 0.101		1.92 ± 0.096		1.638 ± 0.082		1.485 ± 0.074		1.31 ± 0.066		1.248 ± 0.062		1.255 ± 0.063	
K ₂ O	1.495 ± 0.075		1.49 ± 0.074		1.335 ± 0.067		1.059 ± 0.053		0.96 ± 0.048		0.942 ± 0.047		1.040 ± 0.052	
P ₂ O ₅	0.467 ± 0.050		0.452 ± 0.049		0.461 ± 0.050		0.385 ± 0.048		0.446 ± 0.049		0.384 ± 0.048		0.384 ± 0.048	
Total	94.392		98.250		88.192		98.160		87.326		92.503		87.819	
Trace elements (ppm)														
Li	16 ± 1		17 ± 1		19 ± 1		14 ± 1		14 ± 1		13 ± 1		12 ± 1	
V	215 ± 11		157 ± 8		257 ± 13		216 ± 11		283 ± 14		229 ± 11		284 ± 14	
Cr	129 ± 6		94 ± 5		167 ± 8		142 ± 7		177 ± 9		149 ± 7		171 ± 9	
Co	26 ± 1		25 ± 1		29 ± 1		31 ± 2		35 ± 2		36 ± 2		32 ± 2	
Ni	47 ± 2		46 ± 2		53 ± 3		58 ± 3		65 ± 3		61 ± 3		59 ± 3	
Cu	21 ± 1		22 ± 1		24 ± 1		52 ± 3		55 ± 3		58 ± 3		47 ± 2	
Zn	41 ± 2		38 ± 2		44 ± 2		41 ± 2		42 ± 2		42 ± 2		39 ± 2	
Sr	233 ± 13		180 ± 11		381 ± 20		281 ± 15		267 ± 14		259 ± 14		199 ± 11	
Ba	306 ± 15		302 ± 15		404 ± 20		430 ± 21		409 ± 20		407 ± 20		323 ± 16	
Water soluble ions (%)														
Mg ²⁺	0.024 ± 0.001		0.024 ± 0.001		0.026 ± 0.001		0.025 ± 0.001		0.025 ± 0.001		0.025 ± 0.001		0.028 ± 0.001	
Ca ²⁺	0.139 ± 0.018		0.138 ± 0.018		0.126 ± 0.016		0.105 ± 0.018		0.061 ± 0.008		0.081 ± 0.010		0.073 ± 0.009	
Na ⁺	0.019 ± 0.001		0.012 ± 0.000		0.009 ± 0.001		0.008 ± 0.000		0.009 ± 0.001		0.009 ± 0.001		0.019 ± 0.001	
K ⁺	0.016 ± 0.001		0.014 ± 0.001		0.016 ± 0.001		0.016 ± 0.001		0.012 ± 0.001		0.016 ± 0.001		0.018 ± 0.001	
Cl ⁻	0.046 ± 0.002		0.037 ± 0.002		0.026 ± 0.001		0.000 ± 0.002		0.000 ± 0.001		0.000 ± 0.001		0.000 ± 0.001	
SO ₄ ²⁻	0.088 ± 0.001		0.056 ± 0.001		0.038 ± 0.001		0.091 ± 0.001		0.049 ± 0.001		0.070 ± 0.001		0.063 ± 0.001	
PO ₄ ³⁻	0.002 ± 0.001		0.001 ± 0.001		0.000 ± 0.001		0.001 ± 0.001		0.001 ± 0.001		0.001 ± 0.001		0.002 ± 0.001	
NO ₃ ⁻	0.014 ± 0.001		0.009 ± 0.001		0.005 ± 0.001		0.024 ± 0.001		0.012 ± 0.001		0.017 ± 0.002		0.016 ± 0.001	
Mass ratios														
Si/Al	15.370		15.846		12.782		18.628		15.368		13.896		13.705	
Ca/Al	0.367		0.318		0.333		0.389		0.564		0.463		0.511	
Fe/Al	3.097		2.266		3.349		2.858		3.595		2.517		3.127	
Particle diameter from CCSEM measurements (approx. 2000 particles)(µm)														
Geom. Mean (µm)	2.68		2.43		2.55		2.21		2.52		2.63		2.82	
Arith. Mean (µm)	4.50		4.18		4.47		3.67		4.05		4.17		4.94	
Skewness	3.61		3.83		3.63		4.35		4.21		3.93		3.34	
Kurtosis	13.38		14.87		13.14		19.06		18.56		16.74		11.20	
Mean aspect ratio	1.40		1.46		1.43		1.42		1.41		1.43		1.41	